IEEE Access
Multidisciplinary | Rapid Review | Open Access Journal

Received September 25, 2019, accepted October 24, 2019, date of publication November 6, 2019,
date of current version November 15, 2019.

Digital Object Identifier 10.1109/ACCESS.2019.2951819

Design of the Wide Dual-Band Rectangular Souvenir Dielectric Resonator Antenna

XIAO SHENG FANG, (Member, IEEE), AND SHUANG MING CHEN

Department of Electronic and Information Engineering, Shantou University, Shantou 515063, China
Key Laboratory of Digital Signal and Image Processing of Guangdong Province, Shantou University, Shantou 515063, China
Key Laboratory of Intelligent Manufacturing Technology (Shantou University), Ministry of Education, Shantou 515063, China

Corresponding author: Xiao Sheng Fang (fangxs@stu.edu.cn)

This work was supported in part by the National Natural Science Foundation of China under Grant 61701292, in part by the Department of Education of Guangdong Province under Grant 2017KTSCX066, and in part by the STU Scientific Research Foundation for Talents under Grant NTF15008.

ABSTRACT Design of the wide dual-band rectangular souvenir dielectric resonator antenna (DRA) is discussed. The proposed wide dual-band rectangular DRA was excited by using a U-slot. The $TE_{111}{}^{y}$ mode of the rectangular DRA and the slot resonator were employed to design the lower band, while the higher-order $TE_{113}{}^{y}$ and $TE_{311}{}^{y}$ modes were utilized to design the upper band. By merging two pairs of modes in each band, the impedance bandwidth of the lower and upper bands were enhanced simultaneously. New design formulas that determine the dimensions of the wide dual-band rectangular DRA were obtained. Design guideline was also given to facilitate the design. To demonstrate the usefulness of the formulas, a wide dual-band rectangular DRA fabricated using K-9 glass was designed for 2.4/5.2-GHz WLAN applications. To upgrade the antenna as the souvenir-DRA, the word ''LOVE'' was carved on the sidewall of the glass DRA by using the sandblasting machine, and it was found that the content and position of the word has little effect on the antenna performance. The impedance bandwidths of the proposed wide dual-band DRA can be achieved as ∼25% for the lower band and ∼13% for the upper band.

INDEX TERMS Rectangular souvenir dielectric resonator antenna, wide dual-band.

I. INTRODUCTION

Since the study carried out by Long *et al.* [1] in 1983, the dielectric resonator antenna (DRA) [2], [3] has been extensively investigated over the past three decades. The DRA can be rectangular, cylindrical or hemispherical. As compared to the cylindrical and hemispherical ones, the rectangular DRA owns more degrees of freedom, making it more flexible in the parametric selection for designing the bandwidth and mode degeneracy [4], [5].

In recent years, dual-band antennas have been widely employed in modern wireless communications, motivating the studies of the dual-band DRAs. Until now, much work on the dual-band DRAs with directional radiation patterns [6]–[12] have been reported. However, most of them have a relatively narrow impedance bandwidth for one or two frequency bands. For example, a solid DRA that combines a slot resonator was proposed to design the dual-band antenna in [6], but the impedance bandwidth of the lower and upper bands are only ∼2.5% and ∼5.3%. In [12], the fundamental TE_{111} and higher-order TE_{113} modes of the rectangular DRA were employed to design the lower and upper band of the dual-band DRA, respectively. Although the lower-band bandwidth can be achieved as 10.8%, the upper-band bandwidth was only 6.8%. Two methods can be used to achieve the wide dual-band DRA. The first one is to use the hollow DRA [13], [14]. The principle of this method is to reduce the quality factor of the DR, and thus increase its bandwidth. But the processing of this kind of the DRA [13], [14] is relatively difficult since digging hole [13] or trenches [14] in hard media is required. Another method is to employ the triple-mode DRA [15]–[17]. For example, in [15], three DRA modes (quasi-TE_{111}, TE_{113} and TE_{115}) were utilized to realize the wide dual-band CP DRA. In [16], three sets of degenerate orthogonal modes (TE_{111}, TE_{121} and TE_{131}) of the rectangular DRA were excited simultaneously to form a wide dual-band circularly-polarized (CP) DRA. Thus far, however, no analyses have been carried out to determine the dimensions of

The associate editor coordinating the review of this manuscript and approving it for publication was Yang Yang.

the triple-mode DRA when two arbitrary resonance (design) frequencies f_1, f_2 are given. In this article, new results for the design of the wide dual-band rectangular DRA are presented. The proposed wide dual-band rectangular DRA was excited in its $TE_{111}{}^{y}$, $TE_{113}{}^{y}$ and $TE_{311}{}^{y}$ modes by using a U-slot. The $TE_{111}{}^{y}$ mode and the slot resonator were employed to design the lower band, while the higher-order $TE_{113}{}^{y}$ and $TE_{311}{}^{y}$ modes were combined to design its upper band. To facilitate the design, a triple-mode ($TE_{111}{}^{y}$, $TE_{113}{}^{y}$ and $TE_{311}{}^{y}$ modes) engineering formula for the source-free rectangular DRA was firstly derived by using the covariance matrix adaptation evolutionary strategy (CMA-ES) [18]. With the formula, the dimension of the wide dual-band rectangular DRA can be calculated straightforwardly. It should be mentioned that the proposed formula is the first one that considering the three resonant modes of the rectangular DRA, which is the improved version of the dual-mode formulas in [11], [12].

On the other hand, people tend to be afraid of the naked antenna in the sight due to its metallic and radiant effect. Some methods can be used to alleviate this uneasiness. One of them is to hide the antenna in some practical covers like car window [19], rear view mirror [20] and chimney [21], but it has the drawback that the covers would more or less interfere with the normal operation of the antenna. Another method is to use the artistic antenna, such as swan DRA [22], apple DRA [22] and Chinese-character patch antennas [23]–[25]. Compared with the hidden antenna, this kind of the antenna can reduce people's uneasiness without introducing covers. However, its resonance frequency is greatly depended on the shape of the artwork [22] or the Character [23]–[25], which makes the design more difficult. In this article, an easy-to-design artistic rectangular DRA used as the souvenir will be studied. To demonstrate the souvenir-DRA, the word "LOVE" was carved on the sidewall of the DRA by using sandblasting machine. The reflection coefficient, radiation patterns and gain of souvenir-DRA was simulated and measured, and it was found that carving the word has little effect on the antenna performance. The proposed easy-to-design wide dual-band souvenir-DRA can be placed outside without discomfort.

II. TRIPLE-MODE FORMULA OF THE SOURCE-FREE RECTANGULAR DRA

In this part, the triple-mode ($TE_{111}{}^{y}$, $TE_{113}{}^{y}$ and $TE_{311}{}^{y}$ modes) engineering formula for the source-free rectangular DRA was derived. Fig. 1 shows the configuration of a single rectangular DRA locating on a ground plane. The DRA has a length of a, a width of b, a height of d, and a dielectric constant of ε_r. The reason why the $TE_{111}{}^{y}$ and $TE_{113}{}^{y}$ modes were employed is that these two modes can be excited easily, which has been explained in [11]. Here, we explain why the $TE_{311}{}^{y}$ modes is introduced as the third mode in the wide dual-band design. Fig. 2 shows the resonance frequencies of different broadside TE modes of the rectangular DRA as a function of a, which were obtained from the the dielectric waveguide model (DWM) equation [4]. For the design,

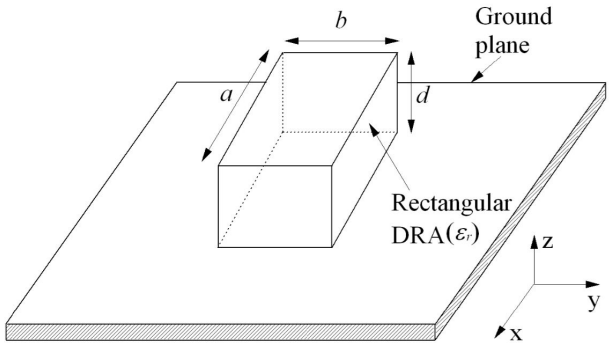

FIGURE 1. Configuration of the source-free rectangular DRA.

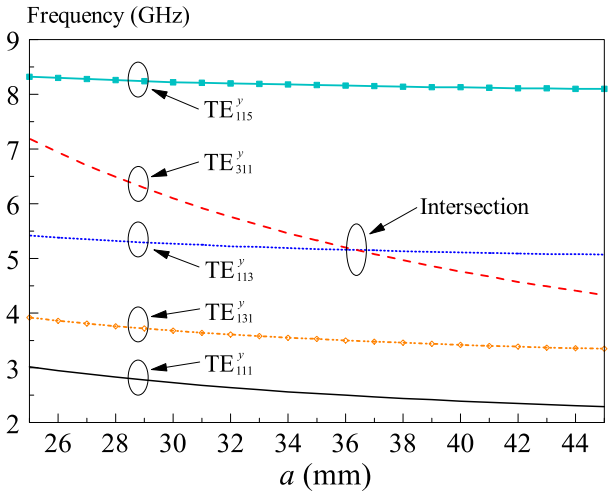

FIGURE 2. Resonance frequencies of different broadside TE modes of the rectangular DRA as a function of a: $b = 34.7$ mm, $d = 18.2$ mm, $\varepsilon_r = 6.85$.

the resonance frequencies of the third mode should be closed to the $TE_{113}{}^{y}$ mode to ensure that they can merge together at the upper band. It can be seen from the figure that the $TE_{311}{}^{y}$ mode is much closer to the $TE_{113}{}^{y}$ mode than the other two higher-order modes ($TE_{131}{}^{y}$ and $TE_{115}{}^{y}$ modes), And therefore, the $TE_{311}{}^{y}$ mode is chosen as the third mode in the wide dual-band design.

Let f_1, f_2 and f_3 be the resonance frequencies of the $TE_{111}{}^{y}$, $TE_{113}{}^{y}$ and $TE_{311}{}^{y}$ modes of the rectangular DRA, respectively. It was found in [12] that the ratio of f_2 to f_1 is independent of dielectric constant, but only related to d/a and b/a, which can be expressed as follows:

$$\frac{f_2}{f_1} = \Phi_1\left(\frac{b}{a}, \frac{d}{a}\right) \tag{1}$$

where Φ_1 is a function of b/a and d/a. On the other hand, the resonance frequencies of the higher-order $TE_{113}{}^{y}$ and $TE_{311}{}^{y}$ modes of the rectangular DRA should be very closed. For simplicity, it is assumed that both modes have the same resonance frequency:

$$f_2 = f_3 \tag{2}$$

By putting (2) into the DWM equation [4], we can obtain:

$$k_{x2}^2 + k_{y2}^2 + k_{z2}^2 = k_{x3}^2 + k_{y3}^2 + k_{z3}^2 \tag{3}$$

where k_{x2}, x_3, k_{y2}, y_3 and k_{z2}, z_3 are the wavenumbers for the $TE_{113}{}^{y}$ and $TE_{311}{}^{y}$ modes along three directions, respectively. Notice that $k_{y2} = k_{y3}$ in DWM equation [4], (3) can be simplified as:

$$k_{x2}^2 + k_{z2}^2 = k_{x3}^2 + k_{z3}^2 \tag{4}$$

By putting $k_{x2} = \pi/a, k_{z2} = 3\pi/2d, k_{x3} = 3\pi/a, k_{z3} = \pi/2d$ into (4), an interesting result can be obtained:

$$\frac{d}{a} = 0.5 \tag{5}$$

Hence, (1) can be simplified as:

$$\frac{f_2}{f_1} = \Phi_3(\frac{b}{a}, 0.5) = \Phi_4(\frac{b}{a}) \tag{6}$$

where Φ_4 is function of b/a. Considering f_2/f_1 are input parameters, (6) is changed to the following form:

$$y = \Phi_5(x) \tag{7}$$

where $x = f_2/f_1$ and $y = b/a$, and Φ_5 is an unknown function to be determined. The DWM was employed to produce numerous data sets for determining Φ_5. It was observed from the data that Φ_5 can be approximated by exponential function as follows:

$$y = \Phi_5(x) \approx \frac{a_1}{e^{a_2 x} + a_3} + a_4 \tag{8}$$

The CMA-ES method was then utilized to find $a_{1,2,3,4}$, which are contained in the 2×2 matrix $\mathbf{A}$ as follows:

$$\mathbf{A} = \begin{bmatrix} a_1 & a_2 \\ a_3 & a_4 \end{bmatrix} \in R^{2\times 2} \quad \text{and} \quad y = \Phi_5(x|\mathbf{A}) \tag{9}$$

An optimal parameter matrix $\mathbf{A_O}$ can be obtained by minimizing the maximum absolute error, and the final optimal parameter matrix was found as follows:

$$\mathbf{A_O} = \begin{bmatrix} 0.0399 & -0.5132 \\ -0.3102 & -0.1854 \end{bmatrix} \tag{10}$$

As designing the wide dual-band DRA, two design frequencies f_1, f_2 and a dielectric constant ε_r is given, and the ratio b/a can be determined from (8) and (10). After obtaining b/a, the length a can be calculated using the single-mode formula (A1) (Appendix), and the width b and height d can be easily obtained from the ratio b/a and d/a. The result can be used over the ranges of $1.8 \le f_2/f_1 \le 2.2$ and $6 \le \varepsilon_r \le 15$, with errors less than 3 %.

It is of interest to know how the dimensions of the triple-mode rectangular DRA vary with the two design frequencies f_1 and f_2. To study this, the design frequencies and dielectric constant are arbitrarily chosen as $f_1 = 2$ GHz, $f_2 = 4$ GHz and $\varepsilon_r = 6.85$. Using our formulas, a, b and d were calculated to be 48.3 mm, 31.1 mm and 24.15 mm, respectively. Fig. 3 (a) shows the percentage change of f_1 corresponding to the percentage changes of a, b and d, with f_2 kept constant. It can be seen from the figure that $|\Delta b| > |\Delta a|$ and $|\Delta b| > |\Delta d|$ are obtained across the range of Δf_1 except at $\Delta f_1 = 0$. The results show that the change of b is larger than for a and d when only f_1 is varied. This indicates that b is more sensitive to f_1 than for a and d. Fig. 3 (b) shows the percentage changes of a, b and d versus the percentage change of f_2, with f_1 kept constant. Similarly, results of $|\Delta b| > |\Delta a|$ and $|\Delta b| > |\Delta d|$ are observed in the range of Δf_2 except at $\Delta f_2 = 0$, which shows that b is more sensitive to f_2 than for a and d. The result is helpful when slightly tuning the frequency in the design.

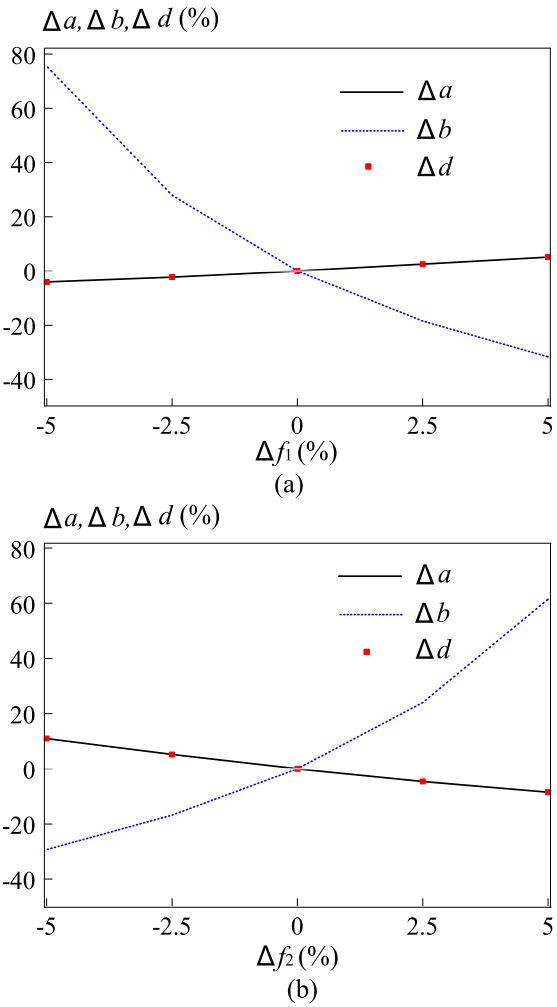

FIGURE 3. (a) Percentage changes of $a(\Delta a)$, $b(\Delta b)$ and $d(\Delta d)$ versus percentage change of f_1 (Δf_1). (b) Percentage changes of a (Δa), $b(\Delta b)$ and $d(\Delta d)$ versus percentage change of f_2 (Δf_2): $\varepsilon_r = 6.85$, $f_1 = 2$ GHz and $f_2 = 4$GHz.

III. DESIGN EXAMPLE

In this part, design example is given to demonstrate the usefulness of the formula. Firstly, the design guideline of the wide dual-band rectangular DRA is summarized as follows:

i) Set the value of the ε_r, f_1 and f_2.
ii) Calculate the ratio b/a using the formula (8) and (10).
iii) Calculate a, b, and d using the formula (A1) (Appendix).

iv) Slightly adjust the ratio d/a to separate two higher-order mode.
v) Adjust the feeding to optimize the impedance bandwidth of the two frequency bands.

Next, the wide dual-band rectangular DRA is designed for 2.4 GHz-WLAN band (2.4-2.485 GHz) and 5.2 GHz-WLAN band (5.15-5.35 GHz) applications, with $f_1 = 2.48$ GHz and $f_2 = 5.15$ GHz. The DRA was fabricated using K-9 glass with a dielectric constant of $\varepsilon_r = 6.85$. Using our result, the dimensions of the DRA were calculated as $a = 36.4$ mm, $b = 34.7$ mm and $d = 18.2$ mm ($d/a = 0.5$). It is worth mentioning that the design formula (8) is obtained under the condition of $f_2 = f_3$. In the practical design, it is preferred to slightly separate f_2 with f_3 so that it can help achieve a wider impedance bandwidth at the upper band. This can be done by slightly increasing the ratio *d/a,* then reducing b to compensate the design frequencies offset (referring to the Fig. 3). The values of $a = 36.4$ mm, $b = 27.1$ mm and $d = 19.2$ mm are used in our final design, with the value of d/a changed from 0.5 to 0.53.

The configuration of the wide dual-band rectangular DRA is shown in Fig. 4.The U-slot feeding method [26] is used to excite the DRA. Here the symmetrical U-slot with a length of L_s, a width of W_s and a protruding length of L_p was used, which was fabricated on the top layer of a substrate having a dielectric constant of $\varepsilon_{rs} = 2.94$, a thickness of $h = 0.762$ mm, and a size of 11×11 cm^2. A 50Ω-microstrip feedline having a width of $W_f = 1.94$ mm and a stub length of $l_s = 6.7$ mm was fabricated on the bottom layer of the substrate.

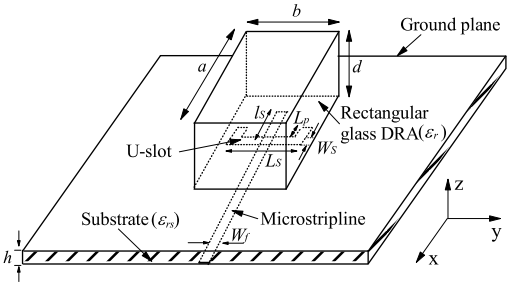

FIGURE 4. Configuration of the wide dual-band rectangular DRA.

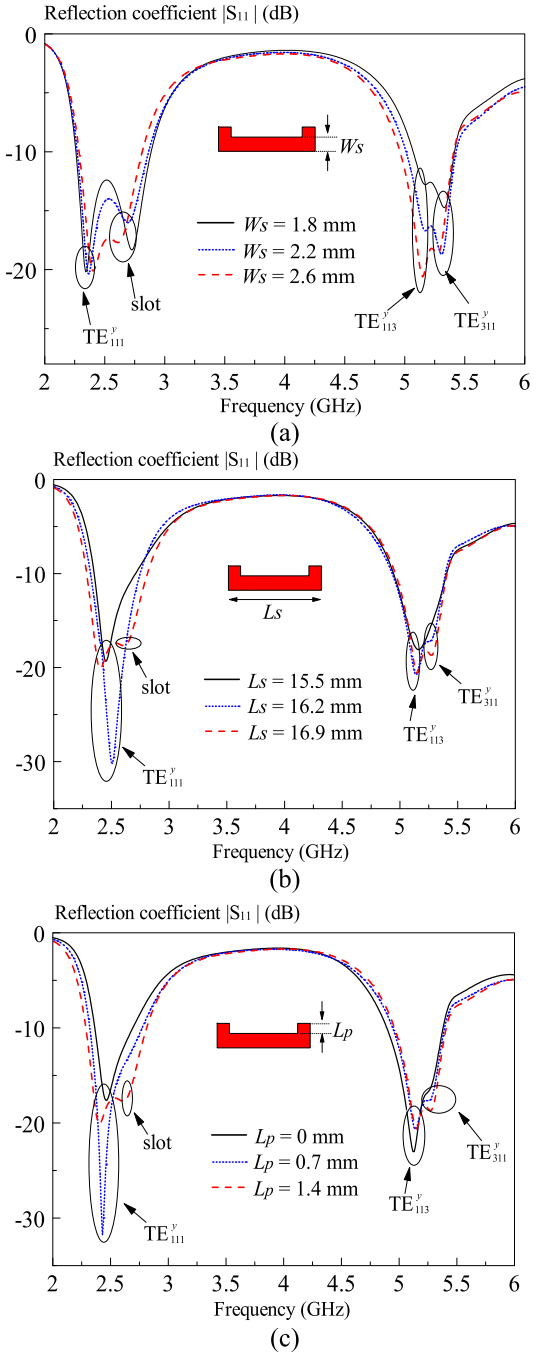

FIGURE 5. Simulated reflection coefficients of the proposed DRA versus frequency: (a) W_S = 1.8, 2.2, and 2.6 mm. (b) L_S = 15.5, 16.2, and 16.9 mm. (c) L_P = 0, 0.7,and 1.4 mm.

The effect of the U-slot dimensions on the reflection coefficient of the proposed wide dual-band rectangular DRA is studied. Fig. 5 (a) shows the simulated reflection coefficient of the DRA as a function of frequency for different W_s. As can be observed from the figure, four resonant modes were observed at around 2.45, 2.6, 5.27 and 5.39 GHz, respectively. The first two resonant modes obtained at the lower-band are due to the $TE_{111}{}^{y}$ mode of the DRA and the slot resonator, and the latter two resonant modes observed at the upper band are caused by the higher-order $TE_{113}{}^{y}$ and $TE_{311}{}^{y}$ modes of the DRA. It was found that increasing W_s can improve the matching level of the upper band but have relatively small effect on that of the lower band. The best result is obtained when $W_s = 2.6$ mm, which is therefore used in our design.

The effect of the slot length L_s on the reflection coefficient is studied in Fig. 5 (b). Three different slot lengths of $L_s = 15.5$ mm, 16.2 mm, 16.9 mm were used. With reference to the figure, increasing the slot length to some extent ($L_s = 16.9$ mm) can excite the slot mode. It merges with the $TE_{111}{}^{y}$ mode of the DRA together, and thus enlarge the

impedance bandwidth of the DRA at the lower band. It can also be seen from the figure that altering the slot length has little effect on the bandwidth of the upper band. In our design, $L_s = 16.9$ mm is chosen.

Fig. 5 (c) shows the simulated reflection coefficient of the DRA as a function of frequency for different L_p. The reason why the U-slot is used in the design is explained here. As can been seen from the figure, when $L_p = 0$ mm, the U-slot is changed as a rectangular slot which provides a relatively narrow impedance bandwidth of the lower band. Increasing L_p can excite the slot resonator and thus enlarge the impedance bandwidth of the lower band significantly. Similarly, altering L_p has relatively small effect on the bandwidth of the upper band. In our design, $L_p = 1.4$ mm is employed.

Based on the results of the parametric study, a wide dual-band rectangular DRA was fabricated by using K-9 glass, with $a = 36.4$ mm, $b = 27.1$ mm, $d = 19.2$ mm, $W_s = 2.6$ mm, $L_s = 16.9$ mm, and $L_p = 1.4$ mm. The prototype of the proposed DRA is shown in Fig. 6 (a) and (b). To demonstrate our souvenir-DRA, the word ''LOVE'' was carved on the sidewall of the DRA by using the glass sand-blasting machine, as shown in Fig. 6 (c). Its production process is summarized as follows: 1) expose the word on the film; 2) stick the film on the glass; 3) spray the word out using the high-pressure gas from the sandblasting machine. Fig. 6 (d) compares the DRAs without and with ''LOVE''. As can been seen from the figure, introducing the word ''LOVE'' makes the DRA more artistic and meaningful.

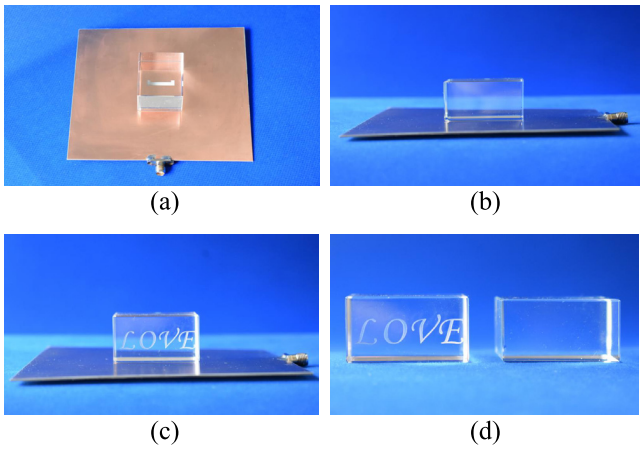

FIGURE 6. Prototype of the wide dual-band rectangular DRA. (a) Top view of the DRA without ''LOVE''. (b) Side view of the DRA without ''LOVE''. (c) Side view of the souvenir-DRA with ''LOVE''. (d) Comparison of the DRAs with and without ''LOVE''.

Fig. 7 shows the measured and simulated reflection coefficients of the proposed DRA without ''LOVE''. With reference to the figure, the measured resonance frequencies (min. $|S_{11}|$) of the $TE_{111}{}^y$, $TE_{113}{}^y$ and $TE_{311}{}^y$ modes of the rectangular DRA are 2.41, 5.18 and 5.33 GHz, respectively, which agree well with the simulated frequencies of 2.38 GHz (1.24 % error), 5.16 GHz (0.39 % error) and 5.28 GHz (0.94 % error). The results also agree reasonably with the

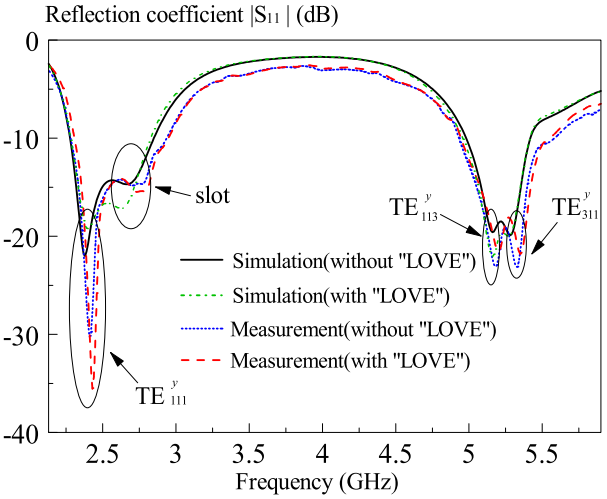

FIGURE 7. Measured and simulated reflection coefficients of the wide dual-band rectangular DRA without/with ''LOVE'' versus frequency: $a = 36.4$ mm, $b = 27.1$ mm, $d = 19.2$ mm, $\varepsilon_{rs} = 2.94$, $h = 0.762$ mm, $W_f = 1.94$ mm, $l_s = 6.7$ mm, $W_s = 2.6$ mm, $L_s = 16.9$ mm, and $L_p = 1.4$ mm.

design frequencies of $f_1 = 2.48$ GHz and $f_{2,3} = 5.15$ GHz. Table 1 lists the measured, design, and simulated frequencies. The errors were calculated referring to the measured results. This result shows the proposed formula is accurate.

TABLE 1. Comparison of measured, design, and simulated resonance frequencies of $TE_{111}{}^y$, $TE_{113}{}^y$ and $TE_{311}{}^y$ modes.

Resonant Mode	Measured frequency (GHz)	Design frequency		Simulated frequency	
		$f_{1,2,3}$ (GHz)	Error (%)	f_{HFSS} (GHz)	Error (%)
$TE_{111}{}^y$	2.41	2.48	2.9	2.38	1.24
$TE_{113}{}^y$	5.18	5.15	0.58	5.16	0.39
$TE_{311}{}^y$	5.33	5.15	3.38	5.28	0.94

The impedance bandwidth of the DRA without ''LOVE'' is discussed next. As can been seen from Fig.7, another resonant mode was observed at 2.41 GHz, which is caused by the U-slot mode. It is exciting to find that the slot mode and the $TE_{111}{}^y$ mode merge together, resulting in a wide impedance bandwidth of the lower band. The measured bandwidth is 24.9 % (2.28-2.93 GHz), completely covering the 2.4 GHz-WLAN band (2.4-2.48 GHz). For the upper band, the $TE_{113}{}^y$ and $TE_{311}{}^y$ modes merge together, resulting in an impedance bandwidth of 12.9 % (4.93-5.59 GHz), which totally covers the 5.2 GHz- WLAN band (5.15-5.35 GHz). Table 2 compares the impedance bandwidths of the present and reported dual-band solid DRAs with directional radiation patterns [6]–[12], [16]. With reference to the table, the bandwidths of the proposed design are wider than those of the reported ones [6]–[12] and comparable to that in [16]. This is reasonable because the proposed design combines a pair of modes at lower and upper bands, respectively. Besides,

TABLE 2. Comparison of bandwidths of different dual-band solid DRAs with directional radiation patterns.

Dual-band solid DRAs	Dielectric constant	Measured 10dB-impedance bandwidths (%)	
		Lower band	Upper band
DRA+Slot [6]	9.8	~2.5	~5.3
DRA+Slot [7]	10	11.8	9.1
Slot+DRA [8]	9.5	~3	~4.8
Slot+DRA [9]	27	9	4.8
DRA+DRA [10]	20	5.8	2.8
Dual-mode DRA [11]	10	15	8.3
Dual-mode DRA [12]	10.8	10.8	6.8
Triple-mode CP DRA [16]	10	27.7	8.5
Triple-mode DRA+Slot (Proposed)	6.85	24.9	12.9

the lower dielectric constant of the glass DRA also helps enlarge the bandwidth.

Fig. 8 shows the simulated E/H-fields of the DRA around the three resonance frequencies. With reference to Fig. 8 (a) and (d), one energy concentration area was found for the $TE_{111}{}^{y}$ mode. For the $TE_{113}{}^{y}$ mode, it theoretically has three standing waves along z-direction. However, only two energy concentration areas along z-direction were found in Fig. 8 (b) and (e), which is due to the existence of the ground plane [11]. For the $TE_{311}{}^{y}$ mode, three energy concentration areas were observed along x-direction in Fig. (c) and (f), as expected. The E/H-field of the slot mode is similar with that in Fig. 8(a) and (d). For simplicity, the result is not include here.

The measured and simulated E/H-plane radiation patterns of the DRA without "LOVE" are shown in Fig.9. As can be observed from the figure, broadside radiation patterns were observed for each mode, which is required for a dual-band antenna. And the co-polarized fields are stronger than the cross-polarized fields by more than 20 dB in the boresight direction ($\theta = 0^{o}$) for both E and H planes, showing that it is a qualified directional antenna.

The measured and simulated antenna gains of the lower band are shown in Fig. 10 (a). As can be observed from the figure, the measured maximum gain caused by the $TE_{111}{}^{y}$ mode was found as 6.05 dBi at 2.38 GHz. Fig. 10 (b) shows the measured and simulated antenna gains of the upper band. With reference to the figure, two peak gains were observed, as expected. The first peak due to the $TE_{113}{}^{y}$ mode was obtained as 7.72 dBi at 5.22 GHz, and the second peak caused by the $TE_{311}{}^{y}$ mode was found as 7.13 dBi at 5.54 GHz. The antenna gain is greater than zero in the whole application frequency bands.

Finally, the wide dual-band rectangular souvenir-DRA with "LOVE" is investigated. For ease of comparison, the simulated and measured reflection coefficient, radiation

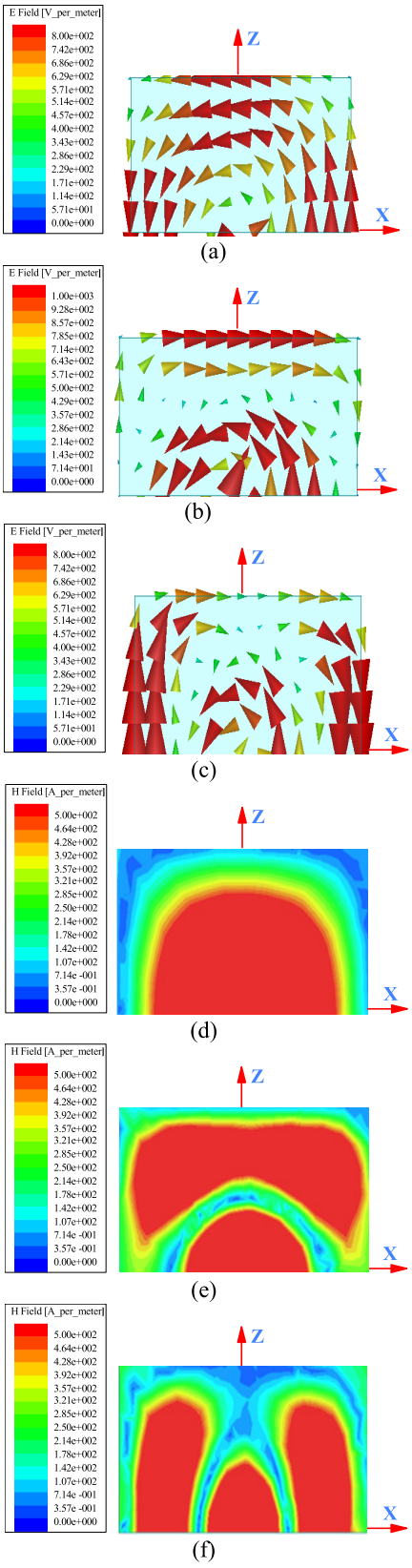

FIGURE 8. Simulated E/H-fields inside the proposed DRA. Parameters are the same as in Fig. 7. (a) E-field of the $TE_{111}{}^{y}$ mode at 2.41 GHz. (b) E-field of the $TE_{113}{}^{y}$ mode at 5.18 GHz. (c) E-field of the $TE_{311}{}^{y}$ mode at 5.33 GHz. (d) H-field of the $TE_{111}{}^{y}$ mode at 2.41 GHz. (e) H-field of the $TE_{113}{}^{y}$ mode at 5.18 GHz. (f) H-field of the $TE_{311}{}^{y}$ mode at 5.33 GHz.

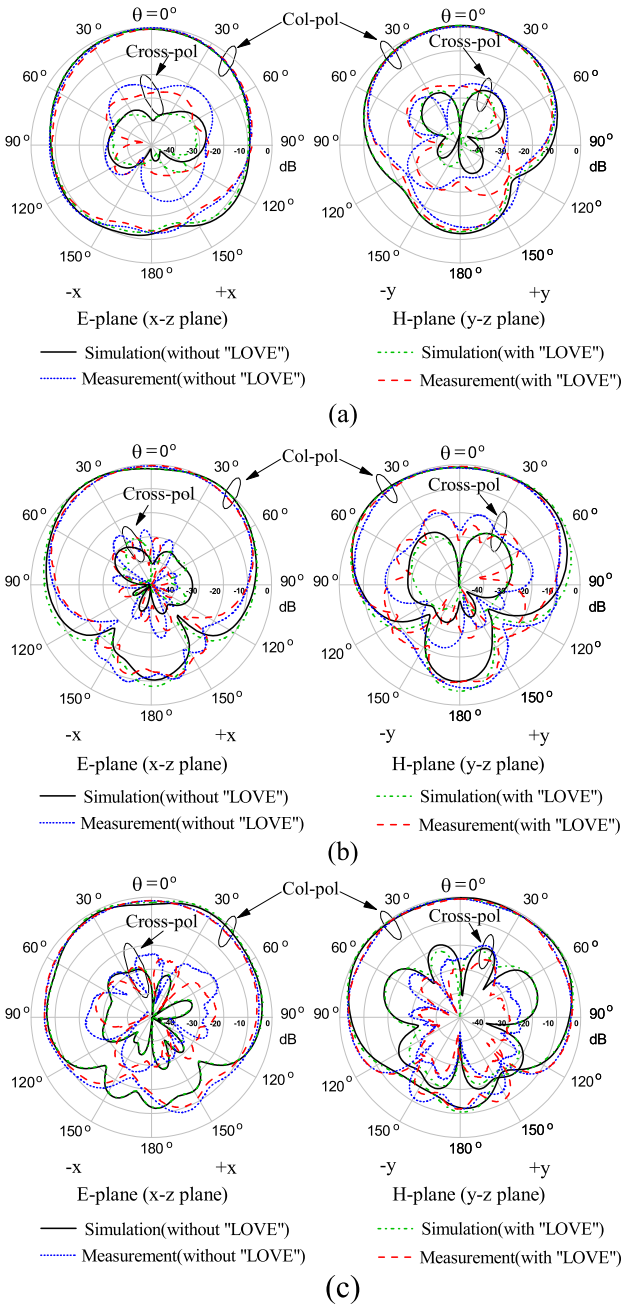

FIGURE 9. Measured and simulated radiation patterns of the wide dual-band rectangular DRA without/with "LOVE". The parameters are the same as in Fig. 7. (a) 2.41 GHz. (b) 5.18 GHz. (c) 5.33 GHz.

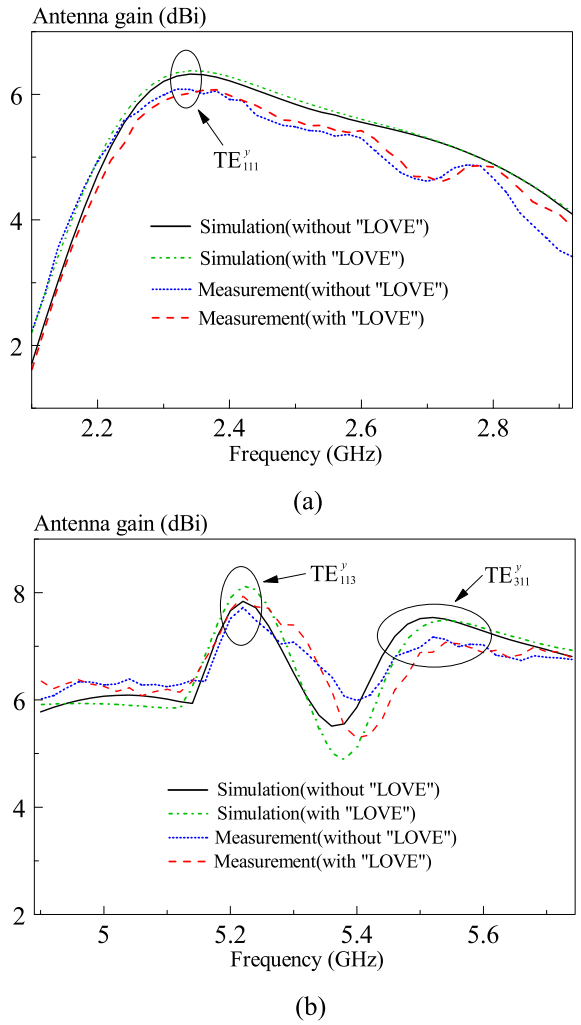

FIGURE 10. Measured and simulated antenna gains of the wide dual-band rectangular DRA without/with "LOVE". (a) Lower band. (b) Upper band. The parameters are the same as in Fig. 7.

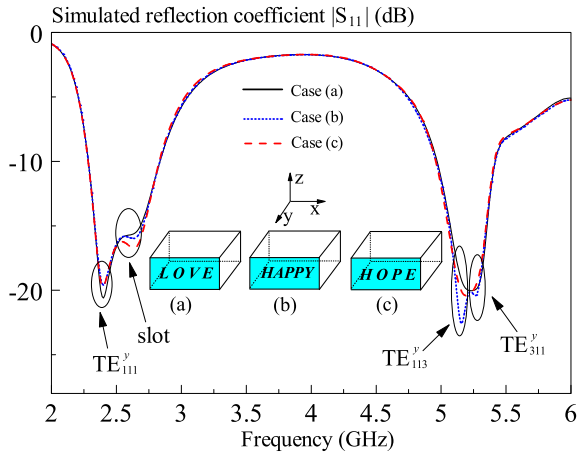

FIGURE 11. Simulated reflection coefficients of the souvenir-DRA with the "LOVE","HAPPY" and "HOPE" carved on the sidewall of the DRA.

pattern, antenna gain of the DRA with "LOVE" are also shown in Fig. 7, Fig. 9 and Fig. 10, respectively. In the simulation, the thickness of the word is set to be 0.3 mm. As can been seen from the figures, the results with and without "LOVE" are basically the same. To further verify the souvenir characteristic, the influence of the content and position of the word on the performance of the DRA is investigated. Fig. 11 shows the simulated reflection coefficients of the souvenir-DRA with the word "LOVE", "HAPPY" and "HOPE" carved at the sidewall of the DRA. As can be seen from the figure, the results are basically the same, showing that the content of the word has little effect on the performance of the antenna. Fig. 12 shows the simulated reflection coefficients

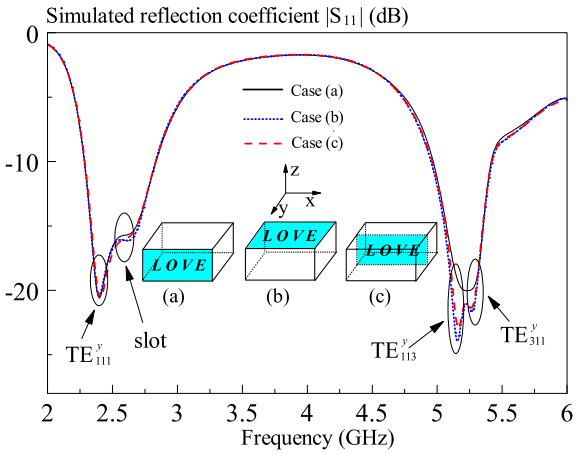

FIGURE 12. Simulated reflection coefficients of the souvenir-DRA with the "LOVE" carved at the side, top and middle of the DRA.

of the souvenir-DRA with the "LOVE" carved at the side, top and middle of the DRA, respectively. The results of the three case are also similar, showing that the position of the word has little impact on the antenna. The radiation pattern and antenna gain of the above cases were also studied and the results were basically the same. For simplicity, the results are not shown here. The above results illustrate that designing the souvenir-DRA is very easy since it is needless to consider the effect of the word.

IV. CONCLUSION

Design of the wide dual-band rectangular souvenir dielectric resonator antenna (DRA) has been studied. The $TE_{111}{}^{y}$ mode of the rectangular DRA and the U-slot resonator have been employed to design the lower band, while the higher-order $TE_{113}{}^{y}$ and $TE_{311}{}^{y}$ modes have been utilized to design the upper band. Engineering formulas that determine the dimensions of the wide dual-band source-free rectangular DRA have been obtained. Using the formulas, a wide dual-band rectangular DRA fabricated using K-9 glass has been designed for 2.4/5.2-GHz WLAN applications. The proposed wide dual-band rectangular glass DRA has an impedance bandwidth of ∼25% for the lower band and ∼13% for the upper band. The word "LOVE" has been carved on the sidewall of the glass DRA by using the sandblasting machine to make it as an souvenir-DRA. It has been found that carving the word on the DRA has little effect on the performance of the antenna. Hence, designing the souvenir-DRA is very easy. The proposed souvenir-DRA can be placed on tables or cupboards without discomfort.

APPENDIX

In [11], an engineering formula is derived to solve the dimension of the rectangular DRA operating at the $TE_{111}{}^{y}$-mode. Given the resonance frequency (f_1) of the $TE_{111}{}^{y}$-mode, the dielectric constant ε_r, the dimension ratios of $q = d/a$ and $p = b/a$, the length a can be calculated using the following formula:

$$a = \frac{c}{2\pi f_1 \sqrt{\varepsilon_r}} \left(\frac{s_1}{s_2 + e^{s_3 p}} + s_4 \right) \tag{A1}$$

where

$$s_1 = -5.29q^4 + 15.97q^3 - 17.74q^2 + 8.812q - 3.198$$
$$s_2 = 0.2706q^4 - 0.7232q^3 + 0.7857q^2 - 0.4558q - 1.023$$
$$s_3 = -8.03q^4 + 23.06q^3 - 24.53q^2 + 11.75q - 3.588$$
$$s_4 = 43.18q^4 - 124.7q^3 + 134.5q^2 - 65.85q + 15.37$$

The above formula is valid over the ranges of $0.4 \le p \le 1$, $0.2 \le q \le 1$, and $6 \le \varepsilon_r \le 100$.

REFERENCES

[1] S. Long, M. McAllister, and L. C. Shen, "The resonant cylindrical dielectric cavity antenna," *IEEE Trans. Antennas Propag.*, vol. AP-31, no. 3, pp. 406–412, May 1983.
[2] K. M. Luk and K. W. Leung, *Dielectric Resonator Antennas*. London, U.K.: Research Studies Press, 2003.
[3] A. Petosa, *Dielectric Resonator Antenna Handbook*. Norwood, MA, USA: Artech House, 2007.
[4] R. K. Mongia and A. Ittipiboon, "Theoretical and experimental investigations on rectangular dielectric resonator antennas," *IEEE Antennas Propag.*, vol. 45, no. 9, pp. 1348–1356, Sep. 1997.
[5] R. K. Mongia, "Theoretical and experimental resonant frequencies of rectangular dielectric resonators," *IEE Proc. H-Microw., Antennas Propag.*, vol. 139, no. 1, pp. 98–104, Feb. 1992.
[6] T. A. Denidni and Q. Rao, "Hybrid dielectric resonator antennas with radiating slot for dual-frequency operation," *IEEE Antennas Wireless Propag. Lett.*, vol. 3, no. 1, pp. 321–323, Dec. 2004.
[7] R. Kumar and R. K. Chaudhary, "A dual-band dual-polarized cubical DRA coupled with new modified cross-shaped slot for ISM (2.4 GHz) and Wi-MAX (3.3-3.6 GHz) band applications," *Int. J. RF Microw. Comput.-Aided Eng.*, vol. 29, no. 1, 2018, Art. no. e21449.
[8] Q. Rao, T. A. Denidni, and A. R. Sebak, "A new dual-frequency hybrid resonator antenna," *IEEE Antennas Wireless Propag. Lett.*, vol. 4, no. , pp. 308–311, 2005.
[9] Y.-F. Lin, H.-M. Chen, and C.-H. Lin, "Compact dual-band hybrid dielectric resonator antenna with radiating slot," *IEEE Antennas Wireless Propag. Lett.*, vol. 8, pp. 6–9, 2008.
[10] Z. Fan and Y. M. M. Antar, "Slot-coupled DR antenna for dual-frequency operation," *IEEE Trans. Antennas Propag.*, vol. 45, no. 2, pp. 306–308, Feb. 1997.
[11] X. S. Fang and K. W. Leung, "Designs of single-, dual-, wide-band rectangular dielectric resonator antennas," *IEEE Trans. Antennas Propag.*, vol. 59, no. 6, pp. 2409–2414, Jun. 2011.
[12] X. S. Fang, C. K. Chow, K. W. Leung, and E. H. Lim, "New single-/dual-mode design formulas of the rectangular dielectric resonator antenna using covariance matrix adaptation evolutionary strategy," *IEEE Antennas Wireless Propag. Lett.*, vol. 10, pp. 734–737, Jul. 2011.
[13] K. W. Leung, X. S. Fang, Y. M. Pan, E. H. Lim, K. M. Luk, and H. P. Chan, "Dual-function radiating glass for antennas and light covers—Part II: Dual-band glass dielectric resonator antennas," *IEEE Trans. Antennas Propag.*, vol. 61, no. 2, pp. 587–597, Feb. 2013.
[14] E. Vinodha and S. Raghavan, "Nine shaped dual wideband rectangular dielectric resonator antenna," in *Proc. Int. Conf. Recent Trends Elect., Control Commun. (RTECC)*, Malaysia, Malaysia, Mar. 2018, pp. 79–82.
[15] M. Zou and J. Pan, "Wide dual-band circularly polarized stacked rectangular dielectric resonator antenna," *IEEE Antennas Wireless Propag. Lett.*, vol. 15, pp. 1140–1143, Oct. 2015.
[16] M. Zhang, B. Li, and X. Lv, "Cross-slot-coupled wide dual-band circularly polarized rectangular dielectric resonator antenna," *IEEE Antennas Wireless Propag. Lett.*, vol. 13, pp. 532–535, 2014.
[17] R. Kumar and R. K. Chaudhary, "Investigation of higher order modes excitation through F-shaped slot in rectangular dielectric resonator antenna for wideband circular polarization with broadside radiation characteristics," *Int. J. RF Microw. Comput.-Aided Eng.*, vol. 28, no. 6, 2018, Art. no. e21281.

[18] M. D. Gregory, Z. Bayraktar, and D. H. Werner, "Fast optimization of electromagnetic design problems using the covariance matrix adaptation evolutionary strategy," *IEEE Trans. Antennas Propag.*, vol. 59, no. 4, pp. 1275–1285, Apr. 2011.
[19] E. Gschwendtner and W. Wiesbeck, "Ultra-broadband car antennas for communications and navigation applications," *IEEE Trans. Antennas Propag.*, vol. 51, no. 8, pp. 2020–2027, Aug. 2003.
[20] K. Yegin, "Diversity antenna system for satellite digital audio radio," *IEEE Trans. Antennas Propag.*, vol. 61, no. 9, pp. 4775–4782, Sep. 2013.
[21] J. Gómez-Yuste, M. Cabedo-Fabrés, E. Antonino-Daviu, and M. Ferrando-Bataller, "Mimetized printed Yagi-Uda antenna array for TDT reception," in *Proc. 11th Eur. Conf. Antennas Propag. (EUCAP)*, Paris, France, Mar. 2017, pp. 3104–3108.
[22] K. W. Leung, E. H. Lim, and X. S. Fang, "Dielectric resonator antennas: From the basic to the aesthetic," *Proc. IEEE*, vol. 100, no. 7, pp. 2181–2193, Jul. 2012.
[23] K. L. Chung, Y. Li, and C. Zhang, "Broadband artistic antenna array composed of circularly-polarized Wang-shaped patch elements," *AEU-Int. J. Electron. Commun.*, vol. 74, pp. 116–122, Apr. 2017.
[24] W. Li, K. L. Chung, R. Liu, and C. Zhang, "A zhong-shaped patch antenna," in *Proc. IEEE Int. Conf. Signal Process., Commun. Comput. (ICSPCC)*, Qingdao, China, Sep. 2018, pp. 1–4.
[25] K. L. Chung, S. Xie, Y. Li, R. Liu, S. Ji, and C. Zhang, "A circular-polarization reconfigurable Meng-shaped patch antenna," *IEEE Access*, vol. 6, pp. 51419–51428, 2018.
[26] B. Li, K. K. So, and K. W. Leung, "A circularly polarized dielectric resonator antenna excited by an asymmetrical U-slot with a backing cavity," *IEEE Antennas Wireless Propag. Lett.*, vol. 2, no. 1, pp. 133–135, 2003.

XIAO SHENG FANG received the B.Eng. degree from Sun Yat-sen University, Guangzhou, China, in 2008, and the Ph.D. degree from the City University of Hong Kong, Hong Kong, in 2012, respectively, all in electronic engineering. From 2012 to 2015, he was a Senior Research Assistant with the Department of Electronic Engineering, City University of Hong Kong. He is currently an Associate Professor with the Department of Electronic Engineering, Shantou University, Shantou, China. His research interests include microwave antennas, dielectric resonator antennas, and passive RF components.

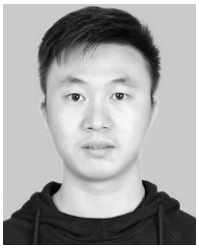

SHUANG MING CHEN was born in Ganzhou, Jiangxi, China, in 1993. He received the B.E. degree in electronics and information engineering from Gannan Normal University, in 2017, where he is currently pursuing the master's degree in engineering with Shantou University. His research interests include dielectric resonator antennas, microwave antennas, and wireless communication.